Comparative Study of Numerical Simulation of External Winding of Arrow-Shaped Wing and Delta Wing

Weijun Feng[1][a], Minghan Wang[2][b] and Menglin Yang[3][c]
[1]*School of Intelligent Manufacturing, Chengdu Institute of Technology, Chengdu, 611700, China*
[2]*School of Mathematics, Statistics and Mechanics, Beijing Institute of Technology, Beijing, 100124 China*
[3]*Yuanxuetong Education Group, Shanghai, 20005, China*

Keywords: Delta Wing, Arrow-Shaped Wing, Numerical Simulation.

Abstract: With the rapid development of the aviation industry, the demand for aircraft performance optimization is increasingly urgent in China. As a new type of aerodynamic layout, the arrow wing has become a key research direction to improve the aerodynamic efficiency of aircraft because of its unique streamlined design and potential drag reduction and efficiency. The objective of this research is to conduct an in-depth exploration of the external flow characteristics of an arrowing within a complex flow field by means of a high-precision numerical simulation approach, thereby providing a scientific foundation for optimizing wing design and enhancing flight performance. In this paper, the computational fluid dynamics (CFD) approach is employed to simulate the external flow features of an arrow wing. As a specially engineered airfoil for aircraft, the arrow wing possesses distinctive aerodynamic performance. Through the establishment of a high-precision calculation model and the application of advanced numerical algorithms, this paper conducts a detailed analysis of the circumfluence phenomena of an arrow wing under various flight conditions. The key parameters, such as velocity field, pressure field, and vortex structure, are compared and analyzed in contrast to the corresponding parameters of the delta wing, thereby obtaining the advantageous aerodynamic conditions of the arrow wing. This provides theoretical guidance for wing topology optimization and scientific basis and technical support for design optimization, aerodynamic performance evaluation, and flow control of arrowing.

1 INTRODUCTION

However, due to its complex flow field structure, it is difficult for traditional experimental methods to fully reveal its circumferential flow characteristics. As an innovative aircraft design concept, the arrow wing has attracted wide attention due to its unique geometry and excellent aerodynamic performance. Therefore, the use of numerical simulation technology has become an important means of studying the external flow around the arrow wing (Gao, 2016) (Zhang, 2010). In this paper, the external flow around the arrow wing is simulated and analyzed in detail based on the CFD method (Yan,2011), and compared with the corresponding external flow around the delta wing simulation data to provide a reference for the research and application in related fields (Li,2016).

2 NUMERICAL SIMULATION METHOD

2.1 Geometric Model and Meshing

This article is first based on the particle size and geometry of the arrow wing, Three-dimensional computational is accurate structured. Soon afterward, this paper used advanced meshing technology, by doing high-quality structuring or unstructured meshing for this arrow wing. The fineness of the mesh has a direct impact on the accuracy of the simulation results, therefore, localized encryption was performed in critical areas (e.g. wingtips, leading

[a] https://orcid.org/0009-0004-2630-1845
[b] https://orcid.org/0009-0008-2767-0799
[c] https://orcid.org/0009-0007-7217-9889

Feng, W., Wang, M. and Yang, M.
Comparative Study of Numerical Simulation of External Winding of Arrow-Shaped Wing and Delta Wing.
DOI: 10.5220/0013444700004558

In *Proceedings of the 1st International Conference on Modern Logistics and Supply Chain Management (MLSCM 2024)*, pages 505-512
ISBN: 978-989-758-738-2

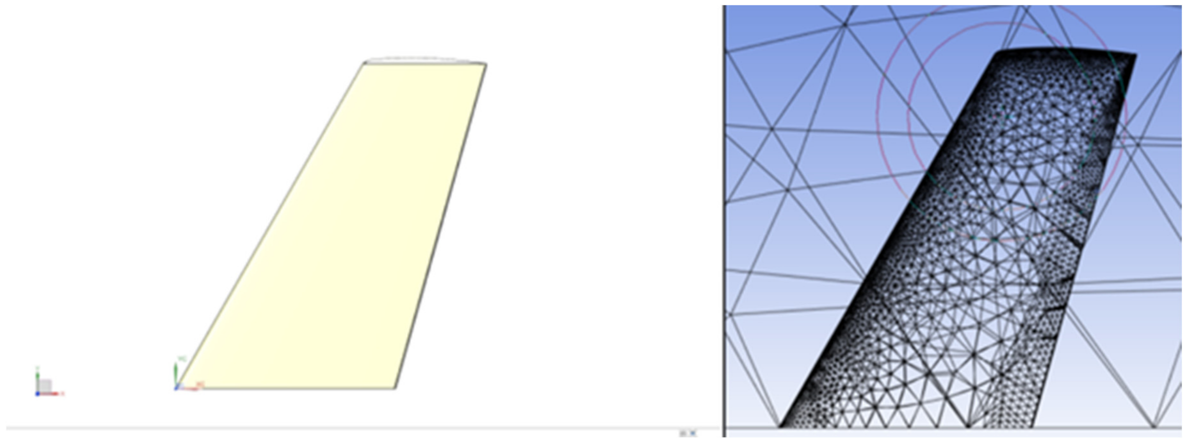

Figure 1: Three views of the tip-wing model and overview of the meshing.

edges,etc.) The breakdown is shown in fig.1 (Han, 2004).

2.2 Numerical Algorithms and Turbulence Modelling

In this paper, a numerical algorithm based on the finite volume method is used, a two-dimensional Reynolds averaged equation (Cheng,2023) (Rumesey,1988) (Spalart,1992).

The continuity equation describes the principle of conservation of fluid mass, in the two-dimensional case it can be expressed as:

$$\frac{\partial \rho}{\partial t}+\frac{\partial(\rho u)}{\partial x}+\frac{\partial(\rho v)}{\partial y}=0 \quad (1)$$

Including, ρ is density, t is time, and u and v are the velocity components of the fluid in the x and y direction.

The momentum equation describes the change in fluid momentum with time and the transfer of momentum due to pressure viscous forces and external forces such as gravity

The momentum equation of two-dimensional RANS can be expressed as:

$$\frac{\partial(\rho u)}{\partial t}+\frac{\partial(\rho u^2)}{\partial x}+\frac{\partial(\rho uv)}{\partial y}=-\frac{\partial p}{\partial x}+\frac{\partial \tau_{xx}}{\partial x}+\frac{\partial \tau_{yx}}{\partial y}+\rho f_x \quad (2)$$

$$\frac{\partial(\rho v)}{\partial t}+\frac{\partial(\rho vu)}{\partial x}+\frac{\partial(\rho v^2)}{\partial y}=-\frac{\partial p}{\partial y}+\frac{\partial \tau_{xy}}{\partial x}+\frac{\partial \tau_{yy}}{\partial y}+\rho f_y \quad (3)$$

Two-dimensional Reynolds averaged equation

Including, ρ is density, τ_{ij} is Components of the viscous stress tensor(i,j=x,y) , f_x and f_y is external force per unit mass in the x and y direction. The viscous stress direction is usually related to the viscous coefficient μ and velocity gradient of the fluid, such as:

$$\tau_{xx}=2\mu\frac{\partial u}{\partial x}+\gamma\left(\frac{\partial u}{\partial x}+\frac{\partial v}{\partial y}\right) \quad (4)$$

$$\tau_{xy}=\tau_{yx}=u\left(\frac{\partial u}{\partial y}+\frac{\partial v}{\partial x}\right) \quad (5)$$

$$\tau_{yy}=2\mu\frac{\partial v}{\partial y}+\gamma\left(\frac{\partial u}{\partial x}+\frac{\partial v}{\partial y}\right) \quad (6)$$

The viscous stress direction including, λ is the second annularity coefficient, for most fluids including gases and water, can be considered as $\lambda=-\frac{2}{3}\mu$.

In the choice of turbulence model, considering the complexity of practicing memory bypassing, the RANS(Reynolds averaged equation) equations, which are suitable for complex flow phenomena, were chosen to be combined with the SST k-ω of the turbulence model for solving. Ensure computational efficiency while better capturing non-stationary and turbulent features in the flow.

2.3 Boundary Conditions and Solution Setup

Reasonable inlet and outlet boundary conditions and surface conditions, as well as the original boundary conditions, are set according to the actual flight conditions of the practice memory Flight state (initial value conditions) : The specified thermodynamic temperature T=300K, is kept constant Mach number M=0.84 corresponds to the computed free-stream velocity $u_{freestream}$ =291.64m/s , Air density ρ=1.148kg/m^3 , corresponds to the computed fluent pressure $p=\rho RT$=9.8858.97Pa

3 SIMULATION RESULTS AND ANALYSIS

3.1 Flow Field Characterisation

The flow field characteristics of an arrow-shaped wing at a given flight speed and angle of attack are obtained through numerical simulation. The results show that the geometry of the arrow-shaped airfoil leads to a unique vortex structure and pressure distribution for its wrap-around flow phenomenon. In the leading edge and wing tip regions, significant vortex separation phenomena occur, and these vortices significantly affect the lift and drag of the wing. The highest static air pressure is found at the leading edge of the wing, with a static ultra-low pressure region at the front at about 1/5 to 2/5 of the airfoil, and a static low-pressure region at 2/5 to 4/5 of the airfoil, and the air pressure in the rest of the wing floats above and below the mean air pressure of the flow field, and the specific distribution of the static air pressure is shown in Fig. 2.

Considering again the nature of the flow field outside the wing, the leading edge of the wing has a relatively slow air flow rate compared to the other regions due to the vortex separation generating region, whereas in the static low-pressure region at the upper edge of the wing at about 2/5 to 4/5 of the airfoil, the airflow rate is generally higher than that at the lower edge, as shown in Fig. 3.

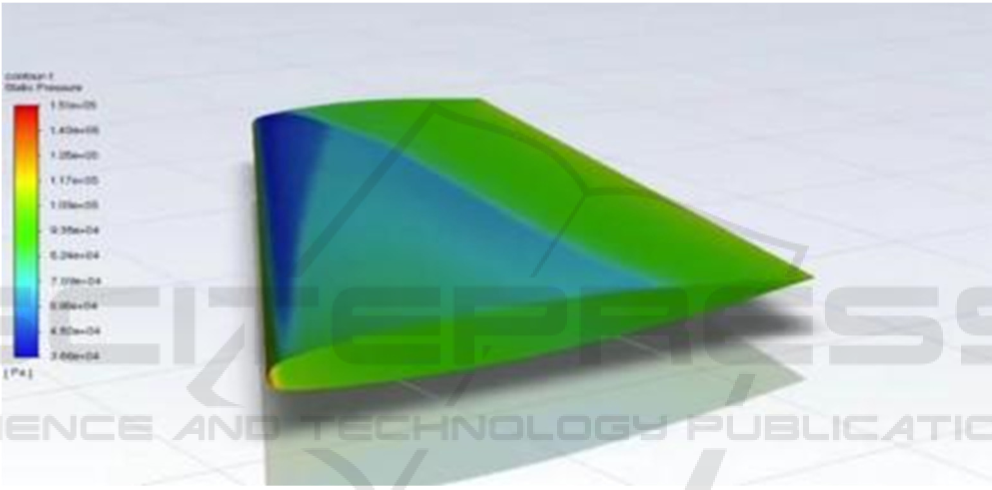

Figure 2a: Arrow airfoil pressure distribution (3D overview).

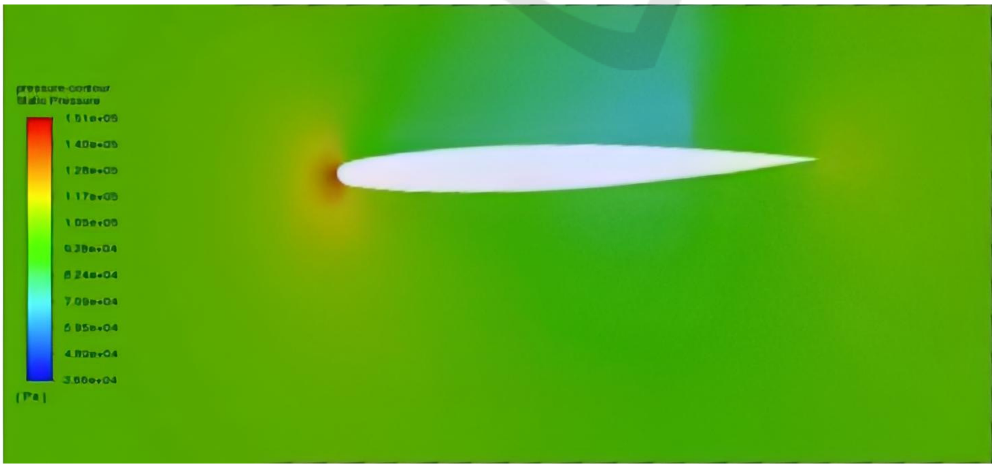

Figure 2b: Arrow airfoil pressure distribution (2D profile).

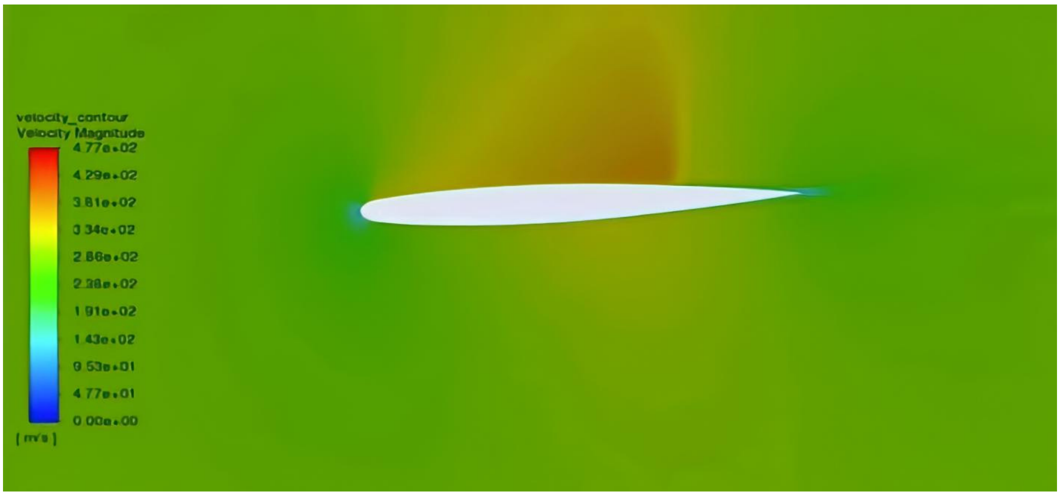

Figure 3: Arrow-shaped wing 2D profile of external bypass flow velocity map.

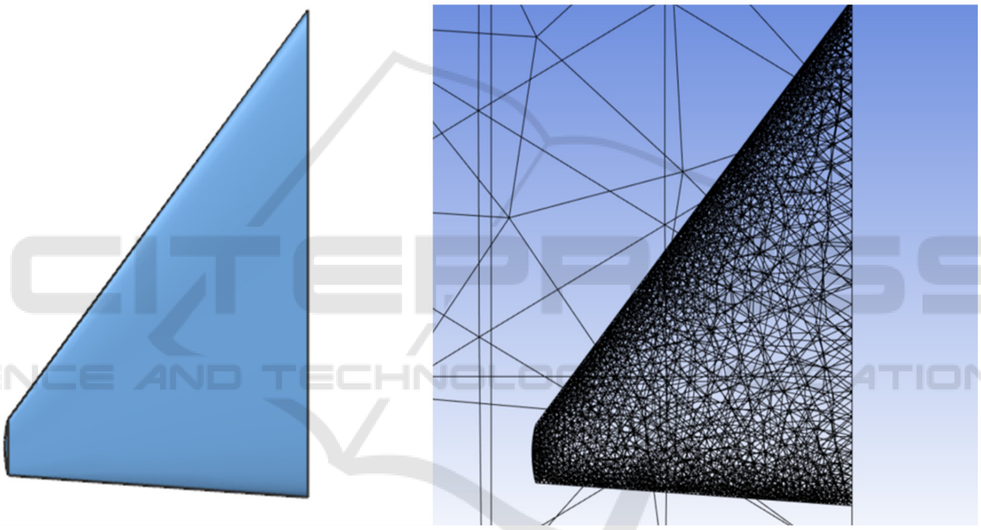

Figure 4: An overview of the three views of the delta wing model used for comparison and its meshing.

3.2 Pneumatic Performance Evaluation (Without Expansion)

Based on the simulation results, the aerodynamic performance of the arrow-shaped wing is evaluated. The key parameters such as lift coefficient and drag coefficient (Yan,2020) were calculated and compared and analyzed with the delta wing (Schaeffler, 1998). In this study, the wing of Mirage 2000 is chosen as the control wing and its meshing with the same conditions as the arrow-shaped wing is shown in Fig. 4.

Subsequently, this study also analysed the pressure distribution of this delta wing with external winding conditions under the same initial value conditions, and the results are shown in Fig. 5.

It is evident from Fig. 6 that the wind drag coefficient (Cd) of the arrow wing, relative to the delta wing, decreases rapidly for the initial few iterations, then gradually levels off and eventually converges at a lower value (the delta wing converges at a higher value). At the beginning of the iterations (about the first 10 iterations), the wind resistance decreases rapidly, from 0.0900 to about 0.0200. after about 40 iterations, the wind resistance stabilizes at about 0.0200. On the contrary, in the first 50 iterations of the delta wing, the wind resistance fluctuates greatly and shows an upward trend, and after about 75 iterations, it gradually decreases from

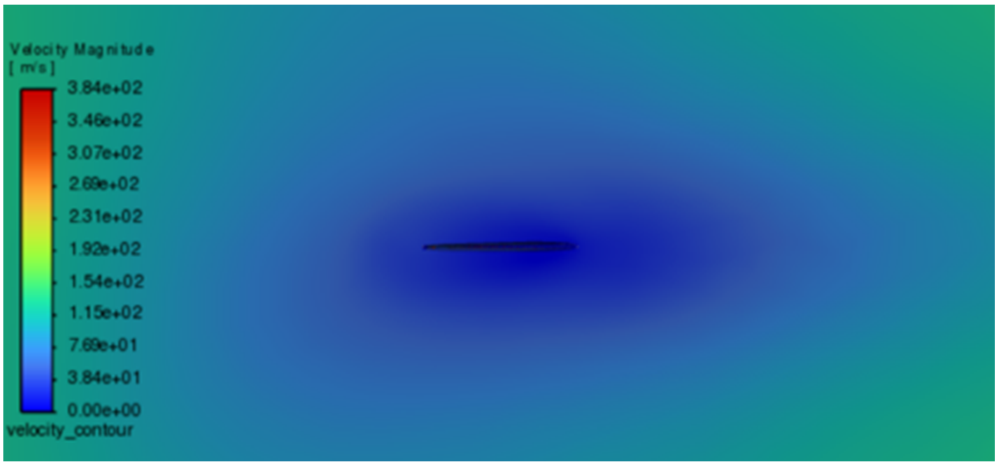

Figure 5a: External bypass flow velocity maps for the delta wing model used for comparison.

Figure 5b: Pressure distribution of delta wing models used for comparison.

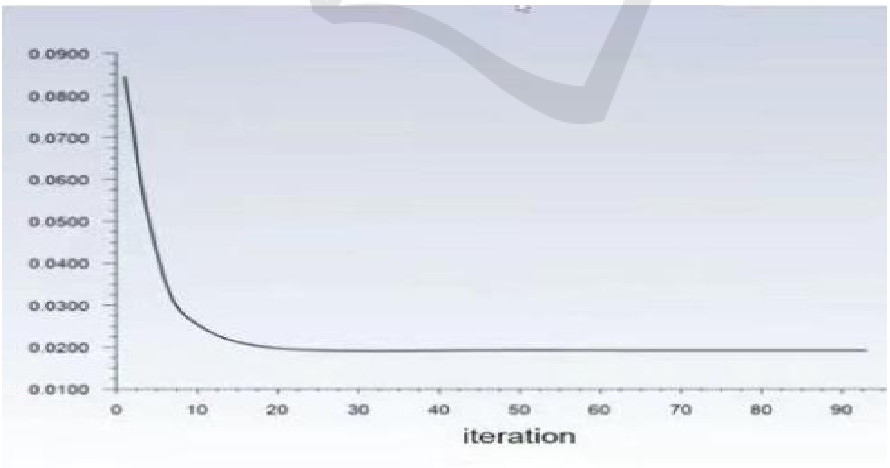

Figure 6a: Variation of wind drag coefficient of the arrow-shaped wing with an increasing number of iterative calculations.

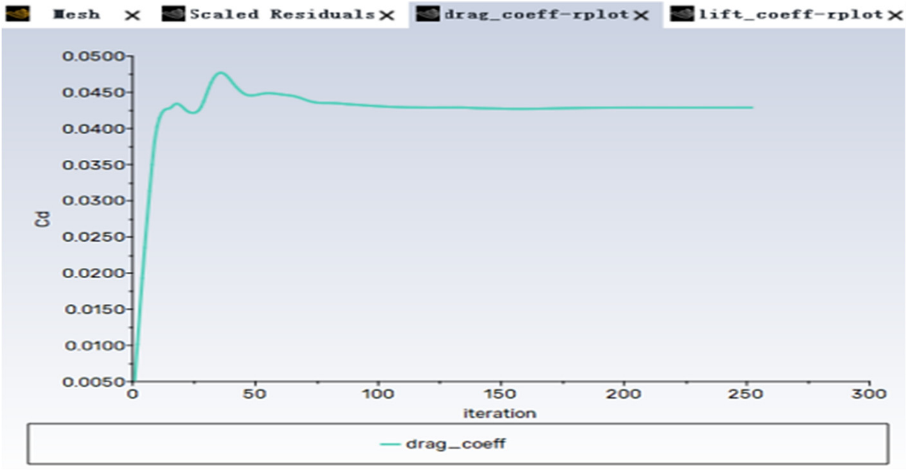

Figure 6b: Variation of wind drag coefficient of a delta wing with an increasing number of iterative calculations.

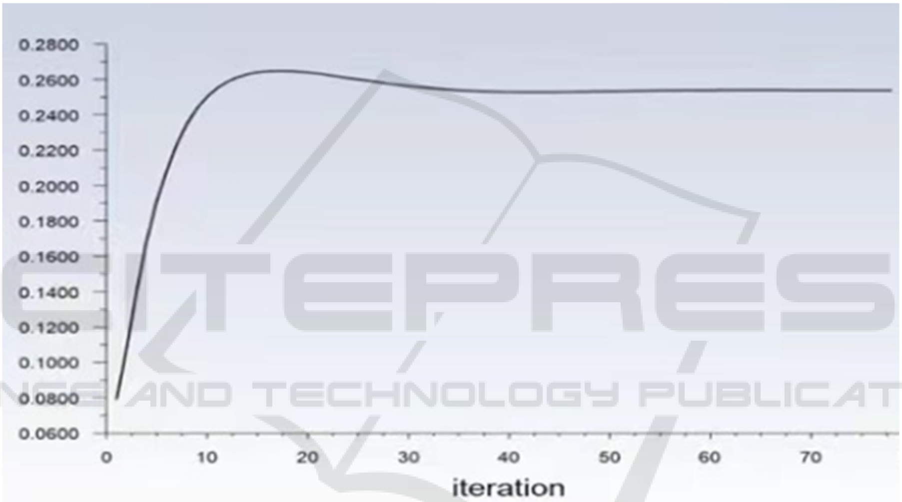

Figure 7a: Variation of lift coefficients of the arrow-shaped wing with an increasing number of iterative calculations.

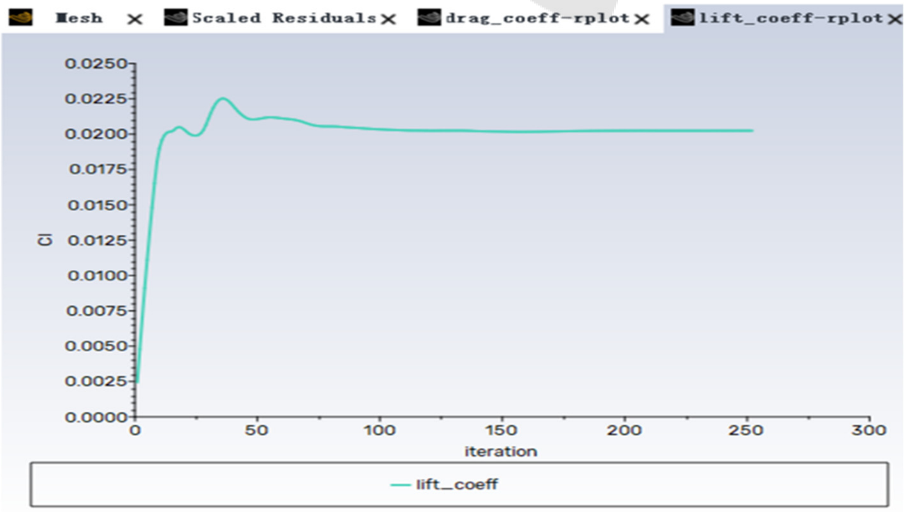

Figure 7b: Variation of lift coefficient of a delta wing with an increasing number of iterative calculations.

0.0475 to about 0.0425 and tends to stabilize, and the wind resistance is higher than that of the arrow-shaped wing

It is obvious from Fig. 7 that, relative to the delta wing, the lift coefficient (Cl) of the arrow wing rises rapidly within the initial 10-step iteration, and there is an increase to a decrease within the 10-step to 20-step iteration, followed by a gradual levelling off, and ultimately converges at a higher value, in the early iteration, the lift coefficient rises rapidly to 0.2620, and then decreases gently to about 0.2500 and stabilises, in contrast to the delta wing, which has a greater fluctuation in the On the contrary, the lift coefficient of delta wing, within the first 50 steps of iteration, fluctuates with a larger amplitude and shows an overall upward trend, and after about 75 steps of iteration, it gradually decreases from 0.0225 to about 0.0205 and tends to be stable, and the lift coefficient is obviously lower than that of the arrow-shaped wing.

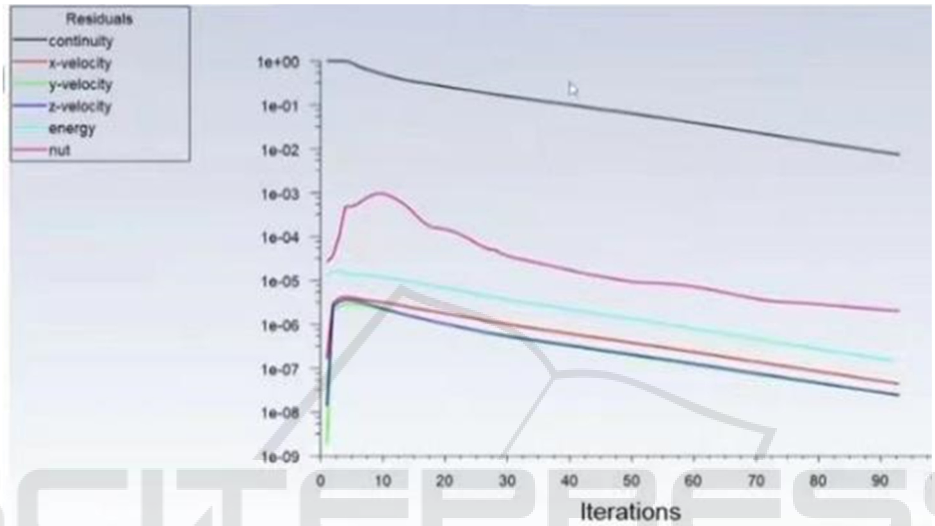

Figure 8a: Variation of the velocity of the arrow-shaped wing with an increasing number of iterative calculations.

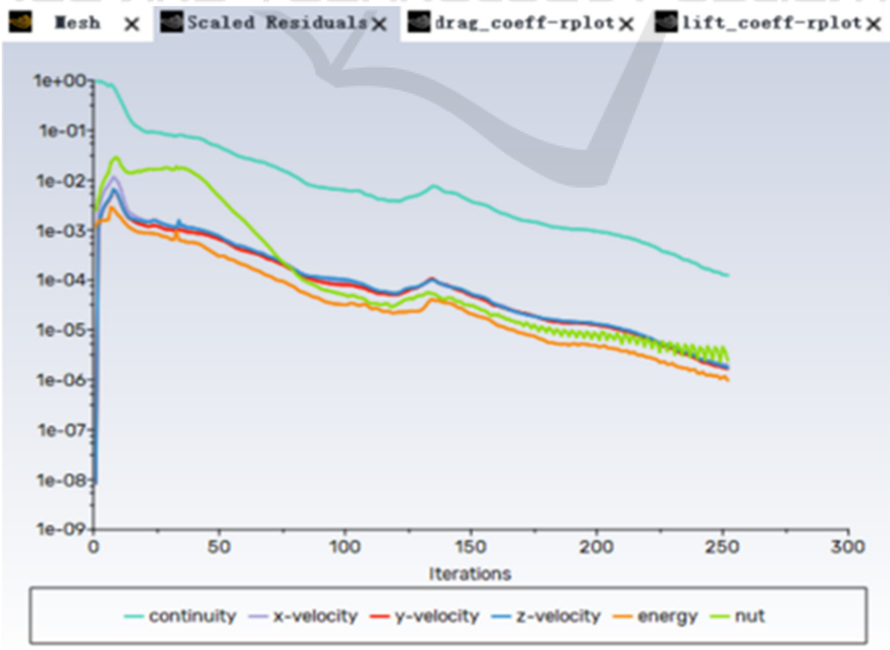

Figure 8b: Velocity of a delta wing with an increasing number of iterative calculations.

It is obvious from Fig 8 that, relative to the delta wing, the lift coefficient (Cl) of the arrow wing rises rapidly within the initial 10-step iteration, and there is an increase to a decrease within the 10-step to 20-step iteration, followed by a gradual leveling off, and ultimately converges at a higher value, in the early iteration, the lift coefficient rises rapidly to 0.2620, and then decreases gently to about 0.2500 and stabilizes, in contrast to the delta wing, which has a greater fluctuation in the On the contrary, the lift coefficient of the delta wing, within the first 50 steps of iteration, fluctuates with a larger amplitude and shows an overall upward trend, and after about 75 steps of iteration, it gradually decreases from 0.0225 to about 0.0205 and tends to be stable, and the lift coefficient is obviously lower than that of the arrow-shaped wing.

4 CONCLUSION

In this paper, the numerical simulation of the external winding flow of an arrow-shaped wing is carried out by CFD method, and the aerodynamic characteristics and flight performance of the arrow-shaped wing and delta wing in a fixed flow field are compared and analysed, and the advantageous flight conditions of the arrow-shaped wing are obtained, which reveal its unique flow field characteristics and aerodynamic performance, and its advantages and disadvantages relative to that of the delta wing. The results provide a scientific basis and technical support for the design optimization, aerodynamic performance evaluation, and flow control of the arrow-shaped wing. In the future, explore more accurate turbulence models, develop adaptive mesh technology, and strengthen the close integration of experimental validation and numerical simulation. to more comprehensively reveal the flow characteristics of the arrow-shaped airfoil and promote the development and application of related technologies.

AUTHORS CONTRIBUTION

All the authors contributed equally and their names were listed in alphabetical order.

REFERENCES

Cheng, J. and Liu, D., Dynamic Flow Field Analysis of a Typical Delta Wing with Large Angle of Approach. *China Flight Test and Research Institute*.

Gao, J., 2016.Numerical simulation of delta wing external winding. *China Academy of Aerospace Aerodynamic Technology*.

Han, Z. and Wang, J., 2004. Examples and Applications of Fluid Engineering Simulation. *Beijing Institute of Technology Press.*

Li, L., 2013.Complex flow field calculation and flow display of 65° delta wing with subsonic velocity. *Aerospace Science and Technology*.

Rumsey, C. and Anderson, W., 1988. Some numerical and physical aspects of unsteady Navier-Stokes computations over airfoils using dynamic meshes. *In 26th Aerospace Sciences Meeting,* 329.

Schaeffler, N. and Telionis, D., 1998. Dynamic delta wing pitchup control via apex flaps. *In 36th AIAA Aerospace Sciences Meeting and Exhibit*, 673.

Spalart, P. and Allmaras, S., 1992. A one-equation turbulence model for aerodynamic flows. Technical Report AIAA - 92-0439. *American Institute of Aeronautics and Astronautics.*

Yan, C., Qu, F., Zhao, Y., et al., 2020. Review and challenges of aerospace CFD physical models and computational methods. *Journal of Aerodynamics*, 38(5): 829-857.

Yan, C., Yu, J., Xu, J., et al., 2011. Achievements in the development of CFD simulation methods. *Advances in Mechanics,* 41(5):562-588.

Zhang, L., Deng, X. and Zhang, H., 2010. A review on the progress of dynamic mesh generation technology and non-stationary computational methods. *Advances in Mechanics,* 40(4):424-447.